Shinshu Med J, 64(3) : 113～121, 2016

Averaging Diffusion-weighted Images Affects the Analysis of the Diffusion Tensor in Vivo

Tomoki KANEKO*, Kikuko KANEKO and Masumi KADOYA
Department of Radiology, Shinshu University School of Medicine

Purpose : The objective of this study was to show an alteration in diffusion tensor indices caused by image averaging.

Materials and Methods : We recruited four healthy volunteers. The diffusion tensor images (DTI) were obtained with non-collinear motion-proving gradients along 12 axes and were repeated 10 times using a 3.0 T MR scanner. The images were averaged in the order of the sessions. The fractional anisotropy (FA), apparent diffusion coefficient (ADC) and eigenvalues (λ1, λ2, λ3) were calculated based on the regions of interest (ROIs) drawn on the commissural, association and projection fibers. To determine the alterations to the FA caused by image averaging, we performed a multiple regression analysis using statistical parametric mapping.

Results : The FA, ADC, λ1 and λ2 values tended to decrease, and the λ3 value tended to increase in proportion to the number of averaging times in the ROI study. In the voxel-based analysis, the FA values significantly decreased proportionally with the increasing number of averaging times.

Conclusions : DTI analysis after image averaging is not desirable because the sharpness of the tensor can be lost.*Shinshu Med J 64 : 113—121, 2016*

(Received for publication October 19, 2015 ; accepted in revised form January 7, 2016)

Key words : diffusion tensor imaging, diffusion weighted image, averaging

I Introduction

In diffusion tensor imaging (DTI), the molecular displacement of the hydrogen nuclei carried by water molecules in the voxel is expressed as a tensor[1]. The diffusion tensor provides unique information about the brain tissue calculated from each voxel of the diffusion-weighted images (DWI)[2]. A series of diffusion-weighted images with bipolar magnetic field gradients, known as the motion-probing gradient (MPG), applied in non-collinear and non-coplanar directions are acquired to calculate the tensor[3)4)]. The characteristic of the tensor is determined using the eigenvalues (e.g., λ1, λ2 and λ3) and other values derived from the eigenvalues, such as fractional anisotropy (FA), relative anisotropy (RA) and volume ratio (VR) [4]. To obtain DWI, fast imaging technology, such as spin-echo echo-planar imaging (SE-EPI), has commonly been used to detect the self-diffusion of water molecules in each voxel[2]. The "single-shot" spin-echo echo-planar sequence is adopted for the acquisition of DWI at one time point using the MPG to confirm the simultaneity of water molecule diffusion. Thus, DWI using the single-shot SE-EPI sequence generates a low signal-noise ratio and is affected by the susceptibility artifact[5].

There are two major methods for improving a low signal-to-noise ratio. One is to increase the number of MPG axes, and the other is to increase the number of times the images are averaged[6)–8)]. The MRI operator must average the images the appropriate number of times and use the appropri-

* Corresponding author : Tomoki Kaneko
Department of Radiology, Shinshu University School of Medicine, 3-1-1 Asahi, Matsumoto, Nagano 390-8621, Japan
E-mail : tk55@shinshu-u.ac.jp

ate number of MPG axes because both methods prolong the total scan time. Although there have been many reports on the relationships between the number of MPG axes and the signal-noise ratio, the influence of the number of times the images are averaged on the DTI indices has rarely been studied. We estimated how the eigenvalues ($\lambda 1$, $\lambda 2$, $\lambda 3$), fractional anisotropy (FA) and apparent diffusion coefficient (ADC) varied with changes in the number of averaging times.

II Materials and Methods

This study was approved by the local ethics committees.

A Subjects

We recruited four participants for this study. All participants were male, and their age ranged from 23 to 53 years (median 24). Informed consent was obtained from each participant. Furthermore, we added a phantom scan to observe unique motion artifacts during the DTI. Details of the structure of the phantom are: ϕ220 mm×135 mm, 5.6 kg, filled with polyvinyl alcohol (PVA) gel material sealed by acrylic plate, meeting the criterion of the American Association of Physicists in Medicine (AAPM) and the National Electrical Manufacturers Association (NEMA) (type 90-401, Nikko Fines industries, Tokyo, Japan).

B MRI acquisition

MR images were acquired using a 3.0 T MR scanner Trio (Siemens, Erlange, Germany) with a 16 ch. head coil. DTI images were obtained using a single shot spin-echo echo-planar sequence in axial orientation. The DTI acquisitions were performed with non-collinear MPGs along 12 axes and were repeated 10 times. Each DTI data set was composed of one reference image (b factor=0) and the following diffusion-weighted images using non-collinear MPGs along 12 axes. The DTI parameters were as follows: repetition time=5300 msec, echo time=90 msec, b factor=1000 s/mm², matrix=128×128, and slice thickness/gap=3/0 mm.

C Image averaging

One radiologist performed image averaging at a built-in console offered by the manufacturer. The set of images obtained at the i (i=1, 2, ..., 10) session was named si. The averaged images (named ni) = (s1+s2+...+si)/i ($2 \leqq i \leqq 10$)・・・Eq. (1). We divided the images into a group of reference images and a group of diffusion-weighted images applying the MPG with the same number of axes. We calculated the "arithmetic mean" of the images using equation (1) above (**Fig. 1**).

D Diffusion Tensor Imaging analysis

The image data (s1, s2, ..., s10, n2, n3, ..., n10) for each subject were analyzed on a stand-alone PC. The following results were obtained using the free software dTV for MR-DTI analysis developed by the Image Computing and Analysis Laboratory, Department of Radiology, The University of Tokyo Hospital, Japan. The dTV software was available via the following URL: http://www.ut-radiology.umin.jp/people/masutani/dTV.htm.

E Data acquisition

1 Scalar value using the region of interest (ROI)

To precisely define the regions-of-interest (ROIs) on the commissural, association and projection fibers, we used the 3 diffusion anisotropy coding (3 DAC) image, which allows the target fiber to be easily recognized on the color-coded map. The two radiologists drew the ROIs corresponding to the fiber tracts on the three DAC images: corpus callosum (CC), cingulum (Ci) and pyramidal tract (Py). Finally, the eigenvalues ($\lambda 1$, $\lambda 2$, $\lambda 3$), fractional anisotropy (FA), and apparent diffusion coefficient (ADC) were obtained from this DTI analysis. In addition to these values, we also calculated the mean of the DTI values of each session in number order. This was an important element of our data analysis because it allowed us to compare the scalar averaging values of each session with the values of the post-image averaging. The eigenvalues of DTI ($\lambda 1$-$\lambda 3$), FA and ADC values are shown in **Fig. 2**.

2 Voxel based analysis

According to the reported (analytical) procedure for voxel-based morphometry using Statistical Parametric Mapping (SPM), we examined the influence of the number of excitations on the FA value.

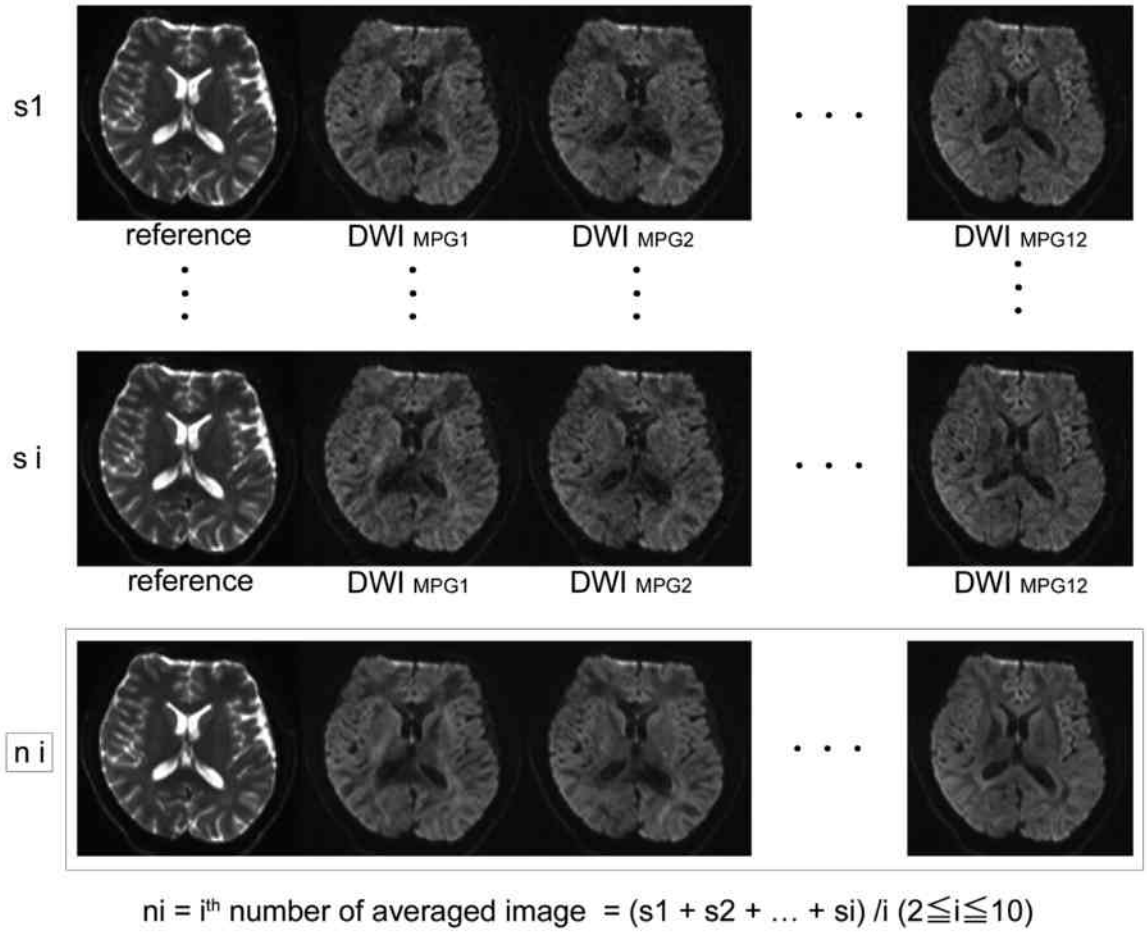

Fig. 1 Method for averaging the diffusion-weighted images for each session. We divided the images into a group of reference images and a group of diffusion-weighted images applying MPG from the same direction. Then we calculated the arithmetic mean of the images using the equation described above (1).

a To assess the FA value, the following procedures were performed[9].

(1) Image preparations : both the reference images and the FA images of all sessions (s1, s2, ..., s10, and n2, n3, ..., n10) were prepared (before the processing step).

(2) Spatial normalization : we normalized the original reference image to the standard space using the "spatial normalization" function of the SPM8, and we obtained the normalization parameter subsequently. Then the FA map was converted to the same space using the obtained normalization parameters.

(3) Making FA template : the arithmetic mean of all of the spatial normalized FA maps was calculated using the image calculator provided with SPM8. The averaged FA map was smoothed adopting an 8 mm filter. Then this smoothed-averaged FA map aided in the development of the new FA template, which was based on the provided FA map.

(4) Re-normalizing : we re-normalized the FA maps directly to the standard space using the smoothed-averaged FA map. This process standardized each FA map to FA template automatically, and enabled the voxel-based analysis throughout the brain.

b Statistical analysis

We estimated the influence on the FA values of 1) the repeated scanning of DTI sessions (s1 to s10) and 2) image averaging (n2 to n10) by using voxel-based analysis of whole brain. We used the multiple regression analysis of the SPM to observe the tendency of FA values, because a linear regression is fitted to the time course of each voxel.

At first, we examined whether the FA values increased or decreased in proportion to the time

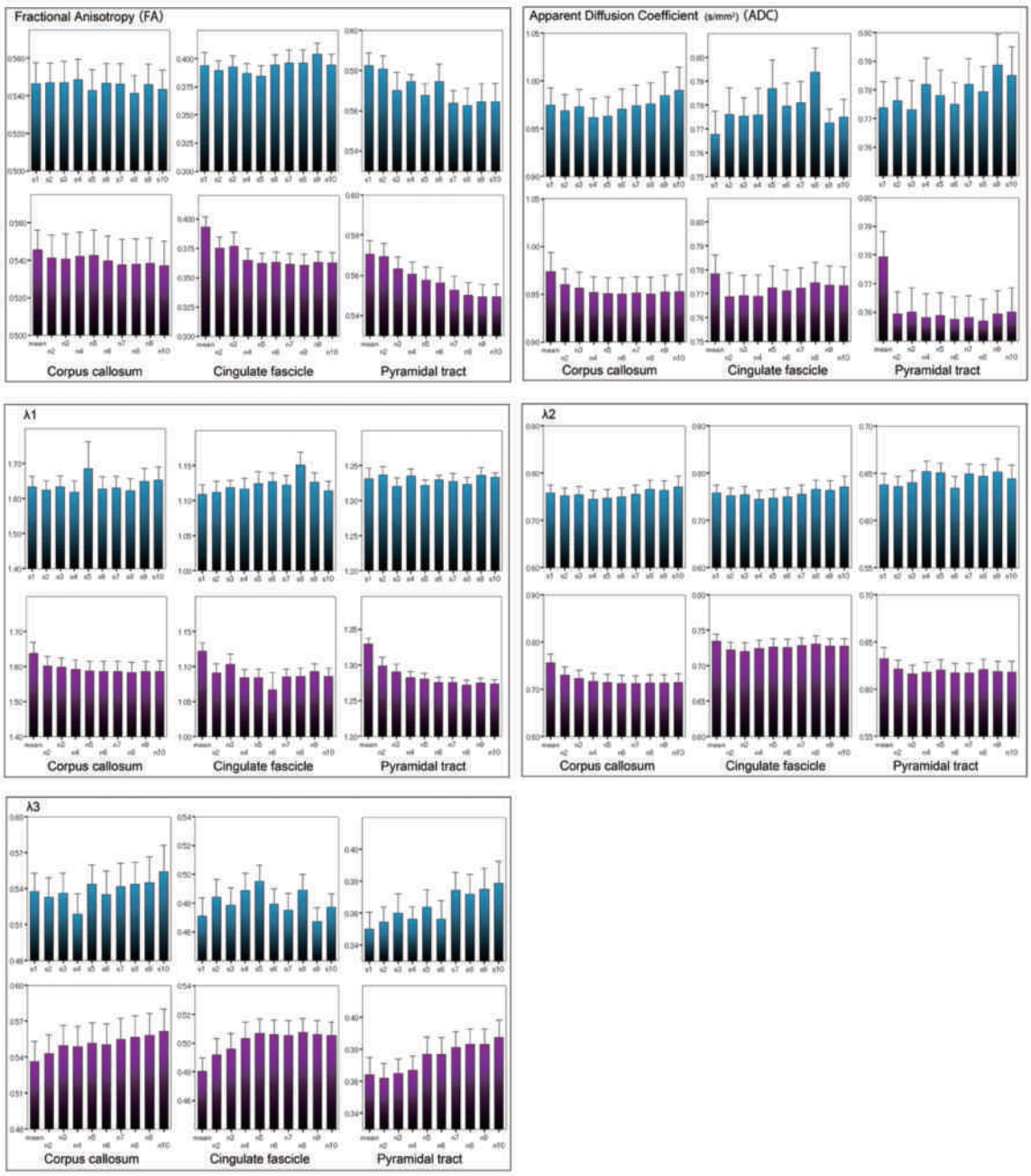

Fig. 2 Diffusion tensor indices (FA, ADC, λ1 to λ3) calculated from the region of interest. Blue columns : "s1 to s10" columns show the values of each session. Purple columns : the "mean" column shows the mean value of all sessions (s1 to s10), and the "n2 to n10" columns show the values of the n^{th} averaged session.

course of sessions (s1 to s10). **Fig. 3 A, B**. Secondly, to estimate the effects of the image averaging, we examined whether the FA values increased or decreased with an increasing number of image averaging times. **Fig. 3 C, D**. To avoid type 1 error, family-wise error (FWE) maintenance was recommended when applying a significance level in SPM. Thus, we adopted FWE management ($p < 0.05$) to make use of the results clinically.

3 Observation of head and phantom rotation

To observe the degree of rotation and the spatial shift of the head and phantom, we executed the "Realign" function of the SPM for all of the b=0 map. The degree of rotation (yaw, pitch, roll) and the spatial shift (x, y, z) during DTI are shown in **Fig. 4**.

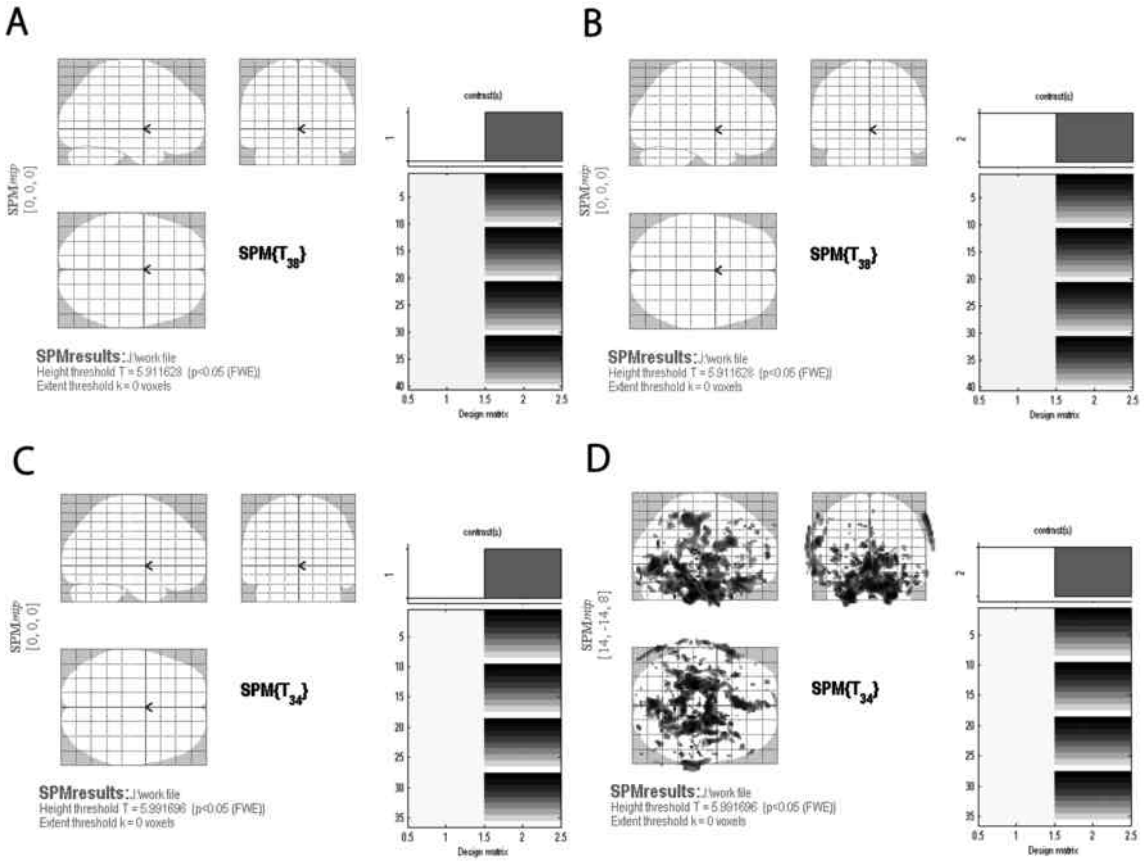

Fig. 3 Voxel-based morphometry for the FA using the SPM. The glass brains are indicated on the left, and design matrix on the right. T value maintained by the family-wise error rate (FWE) is under the glass brains. Gray columns of the upper section of design matrixes show the increase of the FA values examined (upward column) and the decrease of the FA values examined (downward column). The significant voxels are drawn on the glass brain.

Positive (A) and negative (B) correlations of the FA in proportion to increasing number of sessions (s1 to s10) were calculated. Neither a positive nor a negative tendency is shown on either map. In the same manner, positive (C) and negative (D) correlations of the FA in proportion to the increasing number of averaged sessions (n2 to n10) were calculated. Although no positive tendency is shown on map (C), there were multiple coordinates that indicated a negative tendency on map (D).

III Results

In **Fig. 2**, by comparing the ROI data (FA, ADC, $\lambda 1$ to $\lambda 3$) of the scalar averaging of each series (from s1 to s10) to the post-image-averaging (from n2 to n10), we found a tendency of FA, ADC, $\lambda 1$ and $\lambda 2$ to decrease and a tendency of the $\lambda 3$ to increase with an increasing number of image averaging times.

Fig. 3 shows the significant voxels on the glass brain calculated throughout the brain by using voxel-based analysis of SPM. There was no significant increase (**Fig. 3A**) or decrease (**Fig. 3B**) ($t=5.91$, $p<0.05$) between any sessions (s1 to s10). This means the repeated scan would not impinge on the diffusion tensor analysis. On the other hand, multiple significant voxels appeared ($t=5.99$, $p<0.05$) in **Fig. 3D**. This means that the increasing number of averaging times would impact more significantly on the diffusion tensor analysis.

As the scanning time passed, **Fig. 4** shows that the position and the angle of the head from the first-scanned $b=0$ map widened. We were not able to find any kind of tendencies about the head movement. The translations of the phantom were 1/2 or less of the human, and the rotations were 1/5 or less.

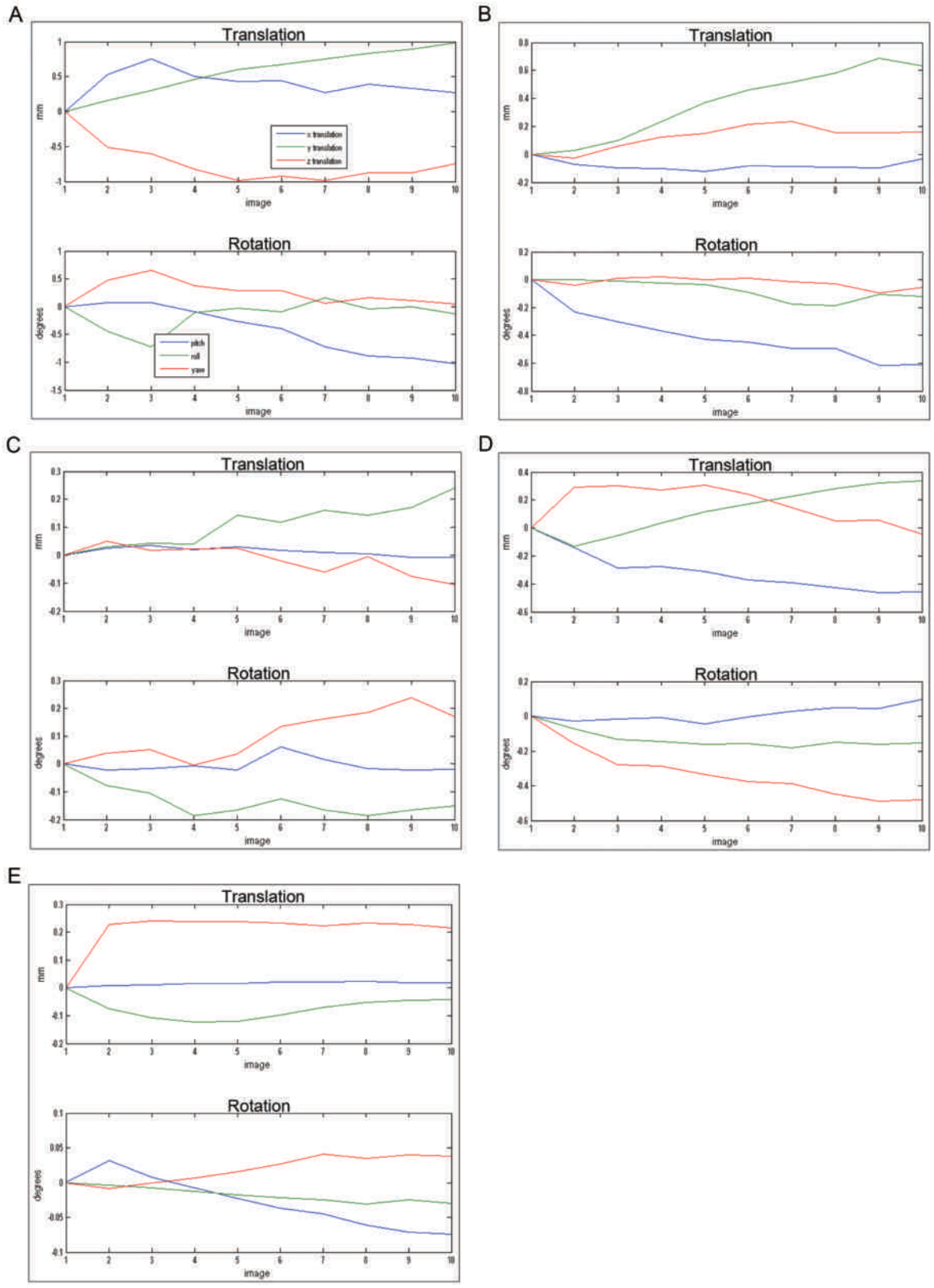

Fig. 4 Variances in the rotation and shift of the head and phantom. A) to D) show the rotation and shift of the head and E) shows that of the phantom.

Ⅳ Discussion

The "single-shot" spin-echo echo-planar sequence made it possible to scan the diffusion-weighted images of the whole brain by applying one bipolar magnetic field gradient. Namely, the SE-EPI sequence showed synchronization of a time phase of the diffusion information of the entire brain[1)–3)]. Conversely, the susceptibility artifact, low signal-noise ratio and eddy current artifact were prominent in comparison with the routine T1/T2-weighted spin-echo sequences[6)].

There are two major methods for improving a low signal-noise ratio. One is to increase the number of MPG axes, and the other is to increase the number of averaging times[6)–8)]. Increasing the number of MPG axes is useful for accurately measuring diffusion tensor because of the phenomenon of fluctuation of water molecule diffusion in vivo[7)10)–12)]. Thus, the applied directions and the number of the axes of the MPG were examined for robust estimation of the DTI[10)11)]. Conversely, the prolongation of the scan time was inevitable when increasing the number of averaging times and MPG axes. The MRI operator had to adopt the appropriate number of averaging times and MPG axes to set the total scan time in an adequate range[6)]. It has been reported that 20 directions of MPG axes for anisotropy analysis and 30 directions of MPG axes for FA analysis generate sufficient conditions for mean diffusibility analysis and the orientation of the diffusion tensor ; however, 20 directions or more of MPG axes are permissible in vivo[6)13)].

In our study, the FA values, $\lambda 1$, and $\lambda 2$ tended to decrease, and $\lambda 3$ tended to increase in proportion to the number of averaging times. The signal of the diffusion-weighted images of the nth session (Sn) was named "Sig Sn", and the signal of the nth averaged image (Nn) was named "Sig Nn". The "Sig Nn" was calculated as follows ;

$$SigNn=\frac{1}{n}\{Sig\ S_1\exp(-b\cdot\overline{{}^t g}\cdot D1\cdot\bar{g})+ Sig\ S_2\exp(-b\cdot\overline{{}^t g}\cdot D2\cdot\bar{g})+\cdots \cdot+Sig\ S_n\ exp(-b\cdot\overline{{}^t g}\cdot Dn\cdot\bar{g})\}$$

Eq. (2)

In our study, as the scanning time passed, the position and the angle of the head dislocated gradually (**Fig. 4**). We were not able to detect any trend or characteristic movement of the translation and rotation among the DTI scans. The rotation angle of the phantom was negligibly small, but the dislocation in the z-axis direction was noticeable as compared with others. Although the phantom was fixed rigidly by filling the gap between the coil and the phantom with gel pads, rostrocaudal (*z*-axis direction) fixation was not conducted. It was considered that the mechanical vibration of the DTI scan induced the dislocation of the phantom between the 1st and 2nd scan, but we were unable to find persistent dislocation after the 2nd scan. Although continuous translation in the phase encoding direction during EPI imaging was reported, we thought that the dislocation of the phantom was just slippage due to mechanical vibration[14)]. As a result, the angle of the diffusion tensor calculated from each session was altered. In addition, the directions of the diffusion tensor of each session might not be uniform because of bulk flow and pulsation in vivo.

If the number of fiber tracts in different orientations, which are approximated based on the tensors with different angular axes, crossed in the voxel, the signal of the diffusion-weighted image (Sig Nn cross) was calculated as follows ;

$$SigNn\ cross=Sig\ S_0\exp\frac{1}{n}\{(-b\cdot\overline{{}^t g}\cdot D1\cdot\bar{g})+ (-b\cdot\overline{{}^t g}\cdot D2\cdot\bar{g})+\cdots \cdot(-b\cdot\overline{{}^t g}\cdot Dn\cdot\bar{g})\}$$

Eq. (3)

$$SigNn\geq SigNn\ cross$$

Eq. (4)

The averaging of the diffusion-weighted signals for each session performed with equation (2) above resulted in the averaging of the tensor having different angular axes, such as crossing fiber tracts (3) (4) ; thus, the diffusion tensor lost its sharpness as the averaging times increased. Adjusting the motion artifact by, for example, shifting and rotating the

head was performed after scanning automatically or manually using the program provided by various researchers. Only adjusting the shift among the diffusion-weighted images appeared to be useful for a robust analysis[15)16)]. However, adjusting the rotation of the head is necessary for adjusting the angular information of the applied MPG direction simultaneously[16)]. The averaging of the image should be calculated using the diffusion-weighted images with the same MPG directions. Adjusting the rotational angle alters the information of the MPG directions; thus, averaging should not be performed on the diffusion-weighted images after rotational angle adjustment. Although image averaging is an excellent procedure for improving the signal-noise ratio, the quality of the averaged image may be decreased by those data affected by substantial motion-induced artifacts during the encoding of the diffusion gradient[17)]. In addition, we recruited healthy participants for this study, and patients are typically more unstable than healthy persons. Furthermore, image averaging causes DTI analysis to lose its sharpness for the tensor and affects the DTI analysis to some extent. Thus, increasing the number of MPG axes and, if possible, adjusting the rotational angle of the applied MPG direction of each diffusion-weighted image are desirable.

Ⅴ Conclusion

DTI analysis using the diffusion-weighted images after image averaging is not desirable because it causes the sharpness of the tensor to be lost.

Ⅵ Limitation

We recruited only four healthy participants for the MR examination. However, when many subjects who are unstable or are not used to MR examination are recruited, we believe that the results will support our current conclusion because more somatic motion of the patients leads to instability of the diffusion tensor.

Ⅶ Conflict of Interest

The authors declare no conflict of interest in this work.

Ⅷ Acknowledgements

We are grateful to Drs. Y. Fujinaga and K. Ueda for assistance in manuscript preparation. We thank Mr. Y. Kito and H. Ueda for providing technical advice.

References

1) Basser PJ, Mattiello J, LeBihan D: MR diffusion tensor spectroscopy and imaging. Biophys J 66: 259-267, 1994
2) Le Bihan D, Mangin JF, Poupon C, Clark CA, Pappata S, Molko N, Chabriat H: Diffusion tensor imaging: concepts and applications. J Magn Reson Imaging 13: 534-546, 2001
3) Basser PJ, Mattiello J, LeBihan D: Estimation of the effective self-diffusion tensor from the NMR spin echo. J Magn Reson B 103: 247-254, 1994
4) Papadakis NG, Xing D, Houston GC, Smith JM, Smith MI, James MF, Parsons AA, Huang CL, Hall LD, Carpenter TA: A study of rotationally invariant and symmetric indices of diffusion anisotropy. Magn Reson Imaging 17: 881-892, 1999
5) Porter DA, Heidemann RM: High resolution diffusion-weighted imaging using readout-segmented echo-planar imaging, parallel imaging and a two-dimensional navigator-based reacquisition. Magn Reson Med 62: 468-475, 2009
6) Ni H, Kavcic V, Zhu T, Ekholm S, Zhong J: Effects of number of diffusion gradient directions on derived diffusion tensor imaging indices in human brain. AJNR Am J Neuroradiol 27: 1776-1781, 2006
7) Poonawalla AH, Zhou XJ: Analytical error propagation in diffusion anisotropy calculations. J Magn Reson Imaging 19: 489-498, 2004
8) Skare S, Li T, Nordell B, Ingvar M: Noise considerations in the determination of diffusion tensor anisotropy.

Magn Reson Imaging 18 : 659-669, 2000
9) Abe O, Takao H, Gonoi W, Sasaki H, Murakami M, Kabasawa H, Kawaguchi H, Goto M, Yamada H, Yamasue H, Kasai K, Aoki S, Ohtomo K : Voxel-based analysis of the diffusion tensor. Neuroradiology 52 : 699-710, 2010
10) Papadakis NG, Murrills CD, Hall LD, Huang CL, Adrian Carpenter T : Minimal gradient encoding for robust estimation of diffusion anisotropy. Magn Reson Imaging 18 : 671-679, 2000
11) Jones DK : The effect of gradient sampling schemes on measures derived from diffusion tensor MRI : a Monte Carlo study. Magn Reson Med 51 : 807-815, 2004
12) Anderson AW : Theoretical analysis of the effects of noise on diffusion tensor imaging. Magn Reson Med 46 : 1174-1188, 2001
13) Papadakis NG, Xing D, Huang CL, Hall LD, Carpenter TA : A comparative study of acquisition schemes for diffusion tensor imaging using MRI. J Magn Reson 137 : 67-82, 1999
14) Foerster BU, Tomasi D, Caparelli EC : Magnetic field shift due to mechanical vibration in functional magnetic resonance imaging. Magn Reson Med 54 : 1261-1267, 2005
15) Muñoz Maniega S, Bastin ME, Armitage PA : Effects of random subject rotation on optimised diffusion gradient sampling schemes in diffusion tensor MRI. Magn Reson Imaging 26 : 451-460, 2008
16) Leemans A, Jones DK : The B-matrix must be rotated when correcting for subject motion in DTI data. Magn Reson Med 61 : 1336-1349, 2009
17) Le Bihan D, Poupon C, Amadon A, Lethimonnier F : Artifacts and pitfalls in diffusion MRI. J Magn Reson Imaging 24 : 478-488, 2006

(2015. 10. 19 received ; 2016. 1. 7 accepted)